Pakistan Veterinary Journal

ISSN: 0253-8318 (PRINT), 2074-7764 (ONLINE)
DOI: 10.29261/pakvetj/2026.109

RESEARCH ARTICLE

Development and Application of Polyclonal Antibody Against S2 Protein of Nephropathogenic Infectious Bronchitis Virus

Zhenni Liu[1#], Yan Shi[1#], Meiqin Wu[1], Cancan Chen[1], Keai Zheng[1], Le Qiu[1], Minghuang Li[1], Xiaona Gao[1], Chao Yin[1]* and Xiaoquan Guo[1]*

[1]Jiangxi Provincial Key Laboratory for Animal Health, College of Animal Science and Technology, Jiangxi Agricultural University, Nanchang 330045, Jiangxi, PR China. [#]The contributions of Zhenni Liu and Yan Shi to this work were equal. *Corresponding author: xqguo20720@jxau.edu.cn; yinc@jxau.edu.cn

ARTICLE HISTORY (26-158)

Received: February 22, 2026
Revised: April 10, 2026
Accepted: April 12, 2026
Published online: April 15, 2026

Key words:
ABCG2
Nephropathogenic IBV
Polyclonal antibody
S2 protein

ABSTRACT

This study examines the S2 protein of the Nephropathogenic Infectious Bronchitis virus (NIBV), essential for the virus's adaptation and expanded tissue and host range. Using bioinformatics, its hydrophilicity, hydrophobicity, signal peptides, antigenic epitopes, secondary and tertiary structures were analyzed. The NIBV-S2 gene was amplified via RT-PCR, cloned into the pET-32a (+) vector to form the recombinant plasmid pET-SX9-S2, and transferred into BL21(DE3) cells. An anti-rHis-S2 polyclonal antibody was generated using the expressed rHis-S2 as the antigen. The indirect ELISA titer of this polyclonal antibody was 1:1024,000. This polyclonal antibody against NIBV-S2 effectively detects NIBV-S2 and is suitable for western bloting, immunofluorescence, and Co-IP experiments. Detection showed a marked rise in NIBV-S2 protein expression from 3 to 9 dpi, peaking at 9 dpi, followed by a decline from 9 to 15 dpi as the infection progressed. At 9 dpi, there was a notable downregulation of the ABCG2, a uric acid transporter, in the kidneys of NIBV-infected chickens compared to the control group. Furthermore, analyses employing molecular docking, immunofluorescence, co-immunoprecipitation (Co-IP), and molecular dynamics (MD) simulations have demonstrated that the NIBV-S2 protein possesses the ability to bind to ABCG2. This observation was further substantiated by in vitro inhibition experiments, which revealed that the expression level of the S protein decreased following the application of the ABCG2 inhibitor Ko143. In summary, NIBV utilizes its S2 protein to interact with ABCG2, thereby facilitating viral colonization in the kidneys, which may contribute to urate accumulation.

To Cite This Article: Liu Z, Shi Y, Wu M, Chen C, Zheng K, Qiu L, Li M, Gao X, Yin C and Guo X, 2026. Development and application of polyclonal antibody against s2 protein of nephropathogenic infectious bronchitis virus. Pak Vet J, 46(5): 1219-1230. http://dx.doi.org/10.29261/pakvetj/2026.109

INTRODUCTION

The Infectious Bronchitis virus (IBV) demonstrates extensive tissue tropism, with the ability to replicate in the epithelial cells of the respiratory tract, kidneys, and oviducts in chickens, thereby inducing multi-systemic damage (Rafique *et al*., 2024; Loor-Giler *et al*., 2025; Uddin *et al*., 2025). Among the various strains, the Nephropathogenic IBV (NIBV) is distinguished by its specific and pronounced affinity for renal tissue (Ying Li *et al*., 2025; Zhang *et al*., 2025). As a member of the Gamma-coronavirus genus, NIBV infection predominantly targets the kidneys, resulting in significant renal impairment and is a principal pathogen responsible for poultry gout (Li *et al*., 2022; Feng *et al*., 2023). The resultant renal damage is characterized by tubular epithelial cell necrosis and inflammation, which are hallmark features of Nephropathogenic Infectious Bronchitis (Liu *et al*., 2022; Shen *et al*., 2023; Qi *et al*., 2024). Consequently, NIBV is associated with notably high mortality rates. Nevertheless, the precise molecular mechanisms underlying its specific renal tropism and the consequent kidney injury remain not fully elucidated.

A pivotal factor influencing viral tissue tropism and pathogenesis is the spike (S) protein, classified as a class I viral fusion protein (You *et al*., 2023). In the case of NIBV, the S protein undergoes cleavage by the Furin protease at the distinct RRSRR site, resulting in the formation of the S1 and S2 subunits (Yamada & Liu, 2009). Post-cleavage, the S2 subunit—encompassing conserved structural elements such as the fusion peptide (FP), heptad repeat regions (HR1 and HR2),

transmembrane domains (TMDs), and the cytoplasmic tail (CT)—assumes a crucial role in facilitating membrane fusion (Bernard *et al*., 2022; Xu *et al*., 2024). During this fusion process, the FP is exposed and integrates into the host cell membrane (Jiang *et al*., 2024), while HR1 and HR2 interact to create a six-helix bundle (6-HB). This configuration brings the viral and cellular membranes into close proximity, thereby facilitating the fusion event (Fan *et al*., 2023). Given its essential role in viral entry, tissue adaptation, and pathogenicity (Mani *et al*., 2025), an in-depth examination of the S2 subunit is imperative to elucidate the molecular underpinnings of NIBV's specific tropism for kidney tissue.

To elucidate the relationship between NIBV-induced renal injury and the functional role of the viral S2 subunit, this study initially conducted a comprehensive bioinformatics analysis of the NIBV S2 protein. This analysis aimed to characterize its physicochemical properties, antigenic epitopes, and secondary and tertiary structures (Chen *et al*., 2024). Building on this foundational work, polyclonal antibodies targeting the S2 protein were developed to facilitate subsequent functional investigations. Specifically, the S2 gene was cloned into the pET-32a(+) vector and expressed as a His-tagged fusion protein in *E. coli* BL21(DE3), which was then used to immunize rabbits. The antibodies generated were subsequently employed to detect S2 expression and localization in NIBV-infected chicks through Western blotting and immunofluorescence techniques.

In the renal system, the ATP-binding cassette transporter ABCG2, predominantly expressed in tubule epithelial cells, is crucial for the excretion of uric acid, functioning through ATP-dependent efflux mechanisms (An *et al*., 2025). Previous research has demonstrated that NIBV infection leads to a downregulation of ABCG2 expression, thereby impairing urate excretion and contributing to renal urate deposition, a significant pathological characteristic of NIBV-associated nephropathy (Chen, Shi, *et al*., 2025). Despite these findings, the specific mechanism by which NIBV suppresses ABCG2 remains inadequately understood, and the potential involvement of the viral spike (S) protein, particularly its S2 protein, in this regulatory process is unclear. In this study, the interaction between the S2 protein and ABCG2 was assessed utilizing molecular docking and molecular dynamics simulations. Concurrently, an immunoprecipitation assay involving S2 and ABCG2 was performed using prepared antibodies. Additionally, an inhibition assay targeting ABCG2 was conducted in primary chicken renal tubular epithelial cells to examine the expression levels of the S2 protein. In conclusion, this study aims to further investigate the interaction between the NIBV S2 protein and host ABCG2, with the objective of determining whether S2 directly or indirectly influences ABCG2 function, thereby promoting renal viral colonization and subsequent disruption of uric acid excretion. Understanding this relationship is anticipated to provide novel mechanistic insights into NIBV-induced renal tropism and the pathogenesis of gout, potentially identifying molecular targets for future therapeutic interventions.

MATERIALS AND METHODS

Animal model creation and sample collection: Two hundred Hy-Line brown chicks, aged 27 days, were allocated into two groups: control check (CK) group and an NIBV infection (NIBV) group. At 28 days of age, the NIBV group was administered with SX9 strain (10^5/0.2 mL) through ocular and nasal routes, whereas the CK group received an equivalent volume of normal saline. Renal tissue samples were harvested from 8 chickens per group at 3, 6, 9, 12, and 15 days post-infection.

Cell culture and treatment: Hy-Line Brown chicks were hatched in incubators, and renal tubular epithelial cells were extracted from 1-day-old chicks. These cells were divided into four groups: Control (standard DMEM), C+Ko143 (DMEM with 10μM Ko143), NIBV (infected with NIBV SX9) and NIBV+Ko143 (infected with NIBV SX9 and treated with 10μM Ko143). All groups were cultured under the same conditions, with regular checks on cell health. Protein samples were taken 36 hours after infection for analysis. Protein samples were taken at 36 hpi for analysis.

Bioinformatics analysis of the NIBV-SX9 S2 gene: The potential signal peptide site of the S2 sequence was analyzed using the sequence data available in GenBank, employing the online analysis software PrediSi. The hydrophilicity and hydrophobicity of the S2 protein sequence were evaluated using the ProtScale online analysis tool. Antigenic epitopes were identified with the DNASTAR software. The tertiary structure of S2 protein was predicted utilizing the online software tool AlphaFold.

Amplification and purification of the S2 gene: RNA was extracted from NIBV-SX9 strain using TRIzol reagent (Vazyme Biotech, China) and reverse transcribed it into cDNA with a TransGen Biotech kit (China). The cDNA template was used to amplify the S2 gene via PCR. The PCR mix included 2μL cDNA, 1μL each of 10μM forward and reverse primers, 12.5μL of Vazyme's 2× Rapid Taq Master Mix and 8.5μL nuclease-free water. Thermal cycling involved an initial denaturation at 94℃ for 5 minutes, followed by 38 cycles of 94℃ for 45 seconds, 56℃ for 30 seconds and 72℃ for 1 minute. Bio-Rad's GelDoc XR system was employed to analyze PCR products on a 1% agarose gel. The amplified DNA fragments were purified using a Vazyme Biotech kit. Both the PCR products and pET-32a (+) vector were double digested with EcoR I and Hind III enzymes. The digested fragments were ligated in a 10μL mixture with 6.5μL of target gene, 1.5μL of vector and 1μL of T4 DNA ligase buffer from Takara Bio Inc.

Construction of expression vectors: Based on the sequence information of the S2 gene, specific primers for the S2 fragment were designed. Using these primers (S2-F: 5'-CCGGAATTCGCCATTGGTCATATGCA-3' (EcoR I); S2-R: 5'-CCCAAGCTTGTAATTGAAGTTGTCAA-3' (Hind III), PCR amplification was performed on the NIBV-SX9 strain, successfully yielding the target S2 segments. The

S2 fragment was then ligated with a vector to construct a recombinant plasmid. This recombinant plasmid was subsequently transformed into the DH5α monoclonal strain. Bacterial tests were conducted using the target gene primers (S2-F/S2-R) and vector primers (P6-F: 5'-CGACGACAAGGCCA TGGCTG-3'; P6-R: 5'-TTAGCAGC CGGATCTCAGTG-3'). Plate of LB agar with ampicillin and incubate at 37℃ for 12 hours. Select a single colony for culture and perform PCR screening to identify positive clones. Send positive samples to Sangon Biotech for sequencing and verify by aligning with the original template. Isolate the confirmed pET-SX9-S2 plasmid and transform it into BL21 (DE3) competent cells according to the guidelines. Repeat as necessary.

Expression of the S2 protein: Bacterial colonies were cultivated until their OD600 reached 0.6-0.8. Then, 1mM IPTG was added to induce expression at 37℃ and 220 rpm for 6 hours to produce the S2 recombinant protein. The protein was analyzed using 10% SDS-PAGE and stained with Coomassie Brilliant Blue R-250 to confirm its presence. After ultrasonic disruption and centrifugation, the supernatant and precipitate were examined via SDS-PAGE to assess protein expression.

Purification of the S2 protein: According to the instructions of the ProteinIsoTM Ni-NTA Resin kit, purify the target protein. An appropriate quantity of medium was resuspended and subsequently introduced into the Ni-NTA 6FF Prepacked Column. Following a period of standing, the 20% ethanol preservation solution was permitted to elute. The column was equilibrated with a volume of the inclusion body equilibration buffer equivalent to eight times the column volume. The inclusion bodies were solubilized in the equilibration buffer, subjected to centrifugation, and subsequently loaded onto the column. The medium was resuspended through repeated pipetting to ensure homogeneity. The system was allowed to stand for 10 minutes to facilitate complete binding. Post-binding, the chromatography column underwent a washing process with the equilibration buffer, incorporating gradient concentrations of 20, 30, 50, 80, 100, 200, 300 and 400 mmol/L. The eluate was collected separately for each gradient elution.

Preparation of polyclonal rabbit anti- S2 protein antibody: Immunize two 2-month-old New Zealand White rabbits, each weighing about 2kg. Before vaccination, collect blood from their ear veins, extract the serum and freeze it at -80℃. The recombinant protein was injected on the 1st, 7th, 14th and 21st days respectively. On day 1, give each rabbit a 1mL dose of recombinant protein at 0.5-1.0 mg/mL, mixed with an equal amount of Freund's complete adjuvant from Sigma-Aldrich, injected subcutaneously. For the next three injections, use the same recombinant protein with Freund's incomplete adjuvant. One week after the final injection, collect more blood from the ear artery, isolate the serum and store it at -80℃.

Enzyme-linked immunosorbent assay: One week after the fourth injection, antibody levels were measured using indirect ELISA. S2 fusion protein was added to microplate wells and incubated overnight at 37℃. After washing, 330 μL of blocking solution was added for 3 hours at 37℃. Rabbit sera (diluted 1:1000 to 1:2048000) were then added and incubated for 1 hour at 37℃. Following another wash, HRP-labeled goat anti-rabbit IgG was added for 1 hour. After a final wash, TMB substrate was added and incubated in the dark for 20 minutes at 37℃. The reaction was stopped with H_2SO_4, and optical density (OD) was measured. A sample was positive if its OD450 was ≥2.1 times the negative serum.

Western blotting: Extract proteins from chicken organs and measure their concentration using Solarbio's BCA Protein Assay Kit, adjusting to 7mg/mL. Separate proteins on a 10% SDS-PAGE gel and transfer to a PVDF membrane. Block the membrane with Epizyme Biotech's solution for 15 minutes at room temperature. Incubate overnight at 4℃ with a 1:1500 dilution of antibody to target S2. Wash the membrane four times with PBST (two 10-minute and two 5-minute washes). Use a 1:5000 HRP-labeled goat anti-rabbit IgG secondary antibody and incubate for 40 minutes at room temperature. Analyze using Abbkine's ELC luminescent liquid and Bio-Rad's ChemiDoc system and process data with Image J software.

Immunofluorescence: All formalin-fixed, paraffin-embedded (FFPE) tissue sections sections were incubated overnight at 4℃ with S2 antibodies. They were then washed with PBST, incubated with secondary antibodies for an hour at room temperature and washed with PBS. TSA was added for 10 minutes, followed by three TBST washes and microwave treatment. DAPI staining was done for 10 minutes at room temperature. After the washing process, sections underwent a five-minute treatment with an autofluorescence quencher, were rinsed and sealed with anti-fluorescence quenching tablets. Results were recorded using confocal microscopy.

Co-immunoprecipitation: For the immunoprecipitation, tissue samples were lysed with an IP lysis buffer containing protease and phosphatase inhibitors. After a 30-minute ice incubation, the lysates were centrifuged at 12,000 rpm for 5 minutes at 4℃ to collect the supernatant. Protein A/G agarose was added to remove nonspecific proteins. The supernatant was then incubated overnight at 4℃ with antibodies against S2 and ABCG2, followed by washing to eliminate nonspecific binding. The final precipitate was analyzed via immunoblotting with primary antibodies for S2 and ABCG2.

Molecular dynamics (MD) simulations: A molecular dynamics simulation of the complex, based on molecular docking, was conducted using Gromacs 2020. The CHARMM36 force field and TIP3P water model were used for the protein and solvation, respectively, with sodium and chloride ions added for charge neutrality. Energy minimization was performed via the steepest descent algorithm. The system was equilibrated under NVT and NPT conditions for 2000 ps, followed by a 100 ns simulation at 300 K, recording trajectories every 10 ps. Analysis included calculating RMSD, RMSF and protein radius of gyration (Rg). Gibbs relative free energy was

determined from RMSD and Rg values, and a free energy landscape map was created with RMSD, Rg and Gibbs free energy on the X, Y and Z axes.

Data analysis: The data analysis was performed utilizing SPSS version 20 and GraphPad Prism version 10.0. Experimental data derived from three independent biological replicates are expressed as the mean ± standard deviation. For comparisons between two groups, unpaired t-tests were applied. The analyses involving multiple groups were performed using a one-way ANOVA, followed by Tukey's post-hoc test. Statistical significance was established at $P<0.05$, with highly significant differences defined as $P<0.01$.

RESULTS

Bioinformatics analysis results of S2 protein: Based on the bioinformatics analysis and protein structure analysis of the S2 protein, the amino acid interval from 810 to 1059 was selected as the prokaryotic expression site of the S2 protein. In order to better understand S2 protein (810 to 1059 aa), a bioinformatics analysis was conducted. As illustrated in Fig. 1A, the overall average hydrophilicity-hydrophobicity index is minus, which means it is a hydrophilic protein. Fig. 1B presents the signal peptide prediction results, which suggest the absence of a signal peptide in the S2 protein. Furthermore, Fig. 1C demonstrates that the S2 protein possesses numerous antigenic epitopes.

Structural analysis of S2 protein: As shown in Fig. 2A, the secondary structure prediction of S2 protein reveals the specific distribution and proportion of its α -helix, extension chain and random coiling. Among them, the α -helix is dominant, containing 119 amino acids, the extension chain accounts for 16%, involving 40 amino acids and the random coiling accounts for 36.4%, containing 91 amino acids. Additionally, the tertiary structure prediction, as depicted in Fig. 2B, confirms that the S2 protein consists of a single polypeptide chain.

Nucleotide sequence analysis of the S2 gene of the NIBV-SX9 strain: The nucleotide sequence of the S2 gene was compared with the relevant reference strains included in GenBank using the MegAlign software in DNAStar (Fig. 3). The S2 gene of the NIBV-SX9 strain has the highest homology with the KM213963.1 strain, at 99.4%, followed by the EF602448.1 strain, at 88.0% and the homology with the remaining strains is 87.0~88%.

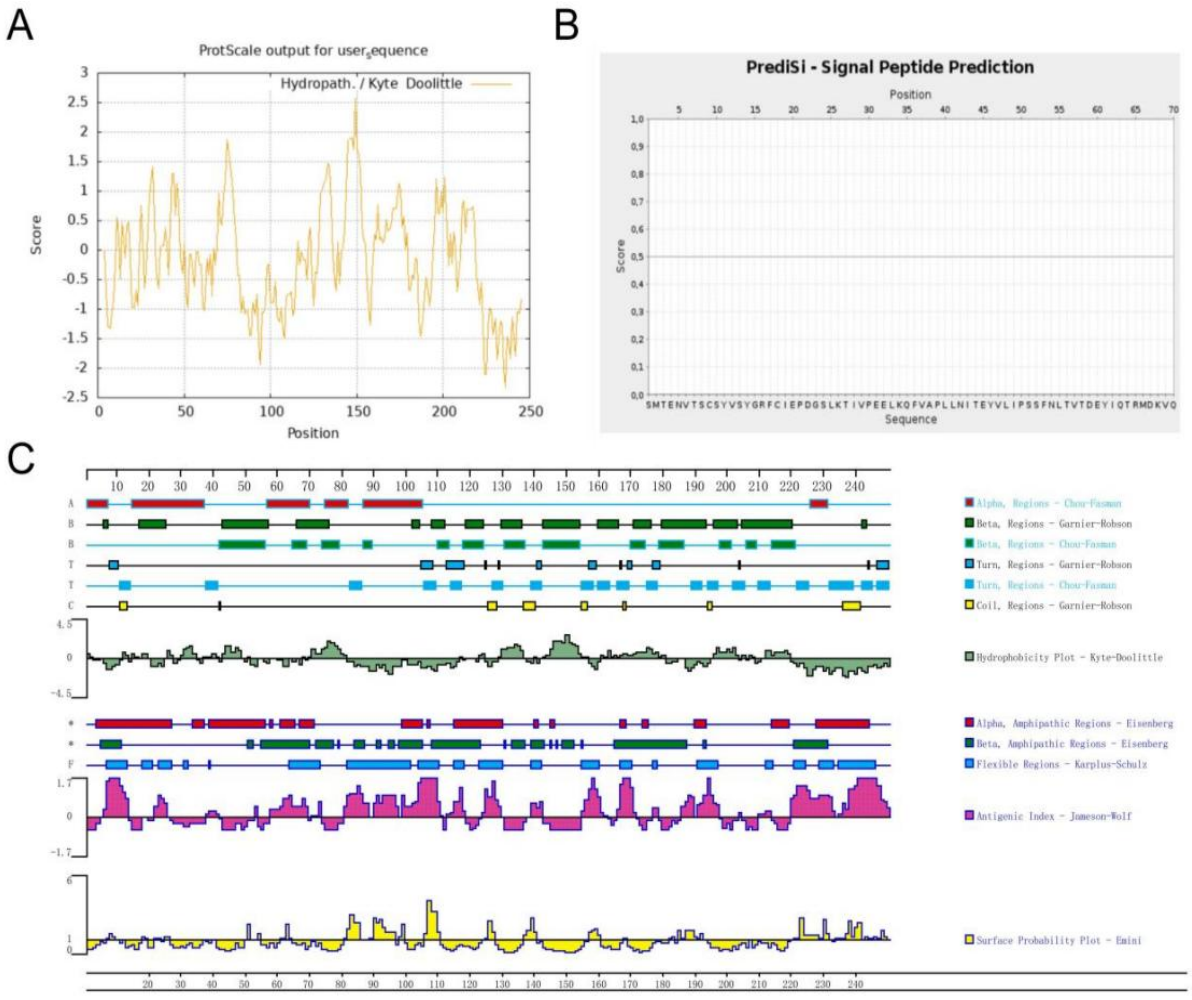

Fig. 1: Bioinformatics examination of NIBV-SX9 S2 protein. A: the predictions for hydrophilicity and hydrophobicity; B: the signal peptide forecasts; C: the antigenic epitopes predictions.

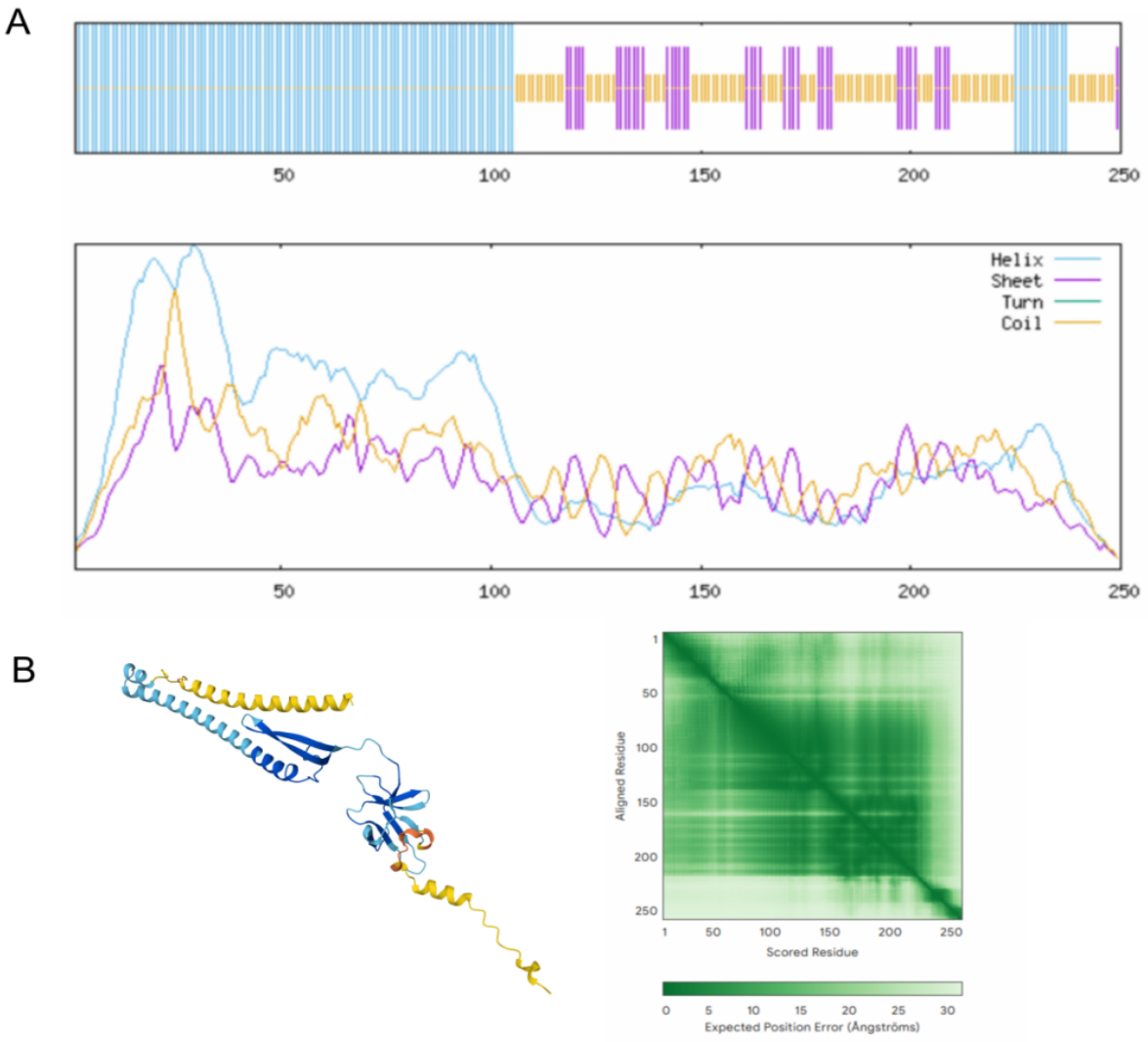

Fig. 2: Structure prediction of NIBV-SX9 S2 protein. A: Secondary structure prediction of NIBV-SX9 S protein. Blue represents α -helix, purple represents Extended strand, and yellow represents Random coil. B: Tertiary structure prediction of NIBV-SX9 S protein.

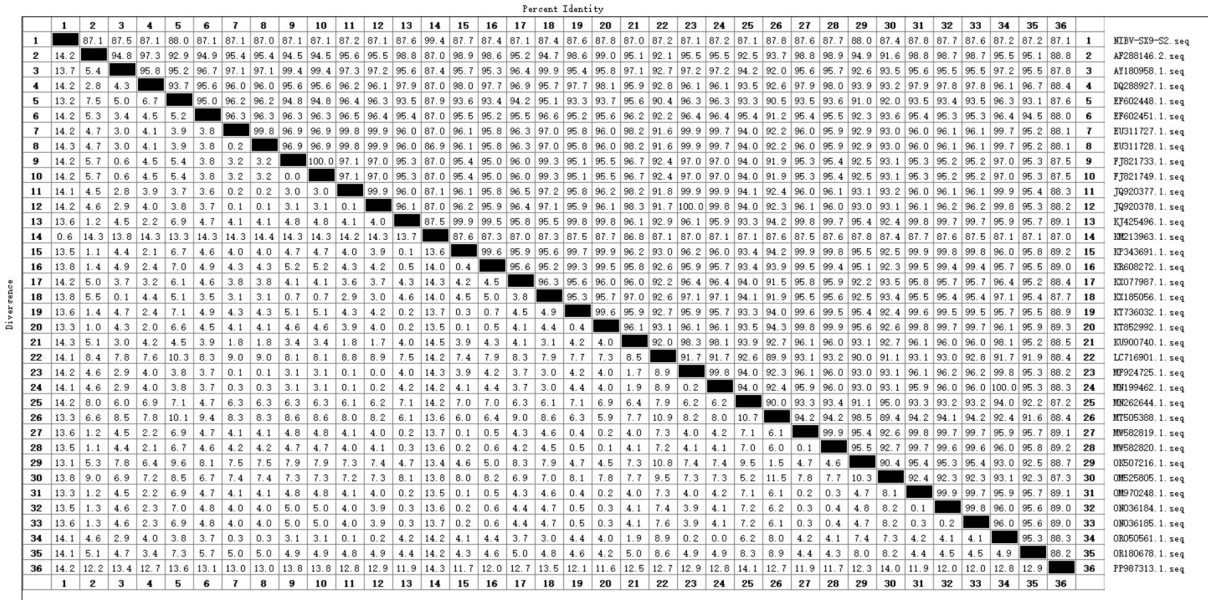

Fig. 3: Nucleotide homology analysis between NIBV-SX9 S2 gene and other strains.

Evolutionary tree analysis of the S2 gene in the NIBV-SX9 strain: Evolutionary tree analysis of the NIBV-SX9-S2 gene showed that different isolates formed two major branches and the NIBV-SX9 strain and the CK/CH/XDC-2/2013 strain (Genebank: KM213963.1) were on one branch (Fig. 4). The rest are all in another major branch and have a relatively distant genetic relationship with the NIBV-SX9 strain of the virus.

Amplification results of the NIBV-SX9-S2 gene and construction of cloning and expression vectors: A 750 bp S2 fragment was amplified from NIBV-SX9 cDNA (Fig. 5A). After ligation into pET-32a(+), transfer to DH5α for amplification, colony PCR using vector primers yielded ~900 bp products, confirming successful insertion (Fig. 5B, lanes 3,5,6). PCR with S2-specific primers further verified the 750 bp target in these colonies (Fig. 5C). The sequencing results obtained from Sangon Biotech Company confirmed correct gene insertion. The recombinant plasmid was transformed into BL21 cells and colony PCR (Fig. 5D, 5E) confirmed its presence, enabling subsequent expression studies.

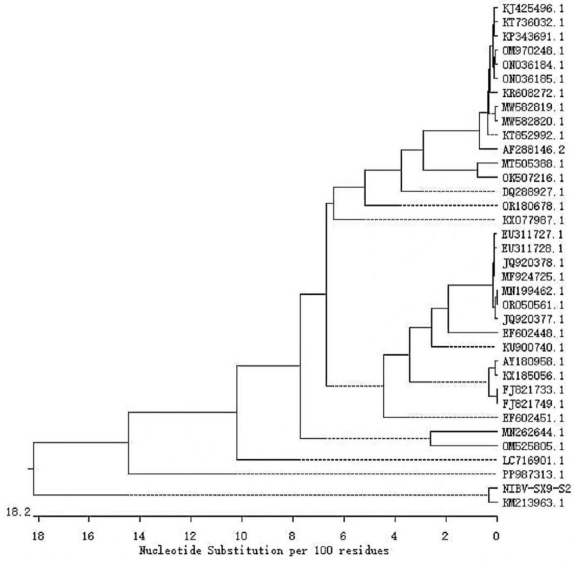

Fig. 4: Phylogenetic tree analysis between NIBV-SX9 S2 gene and other strains.

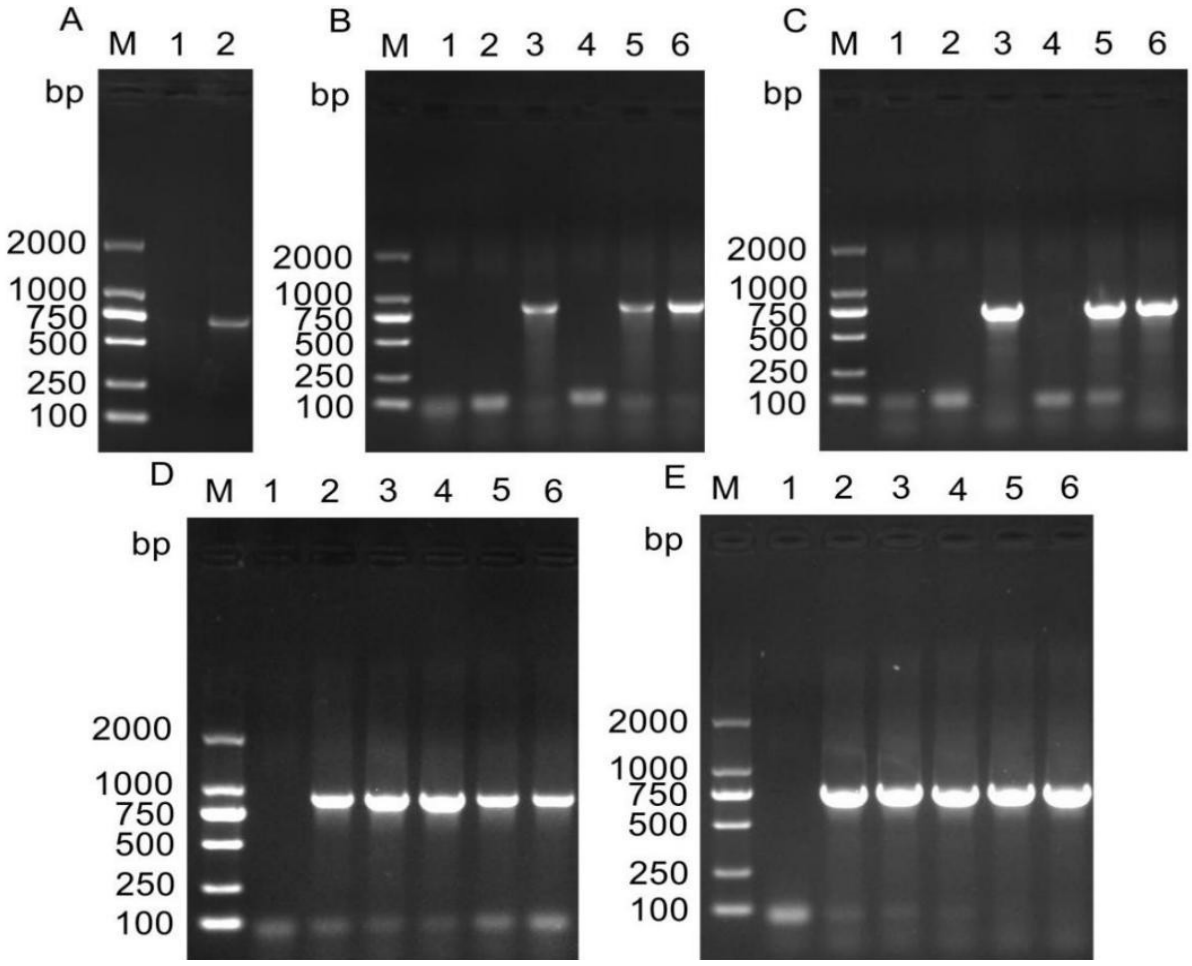

Fig. 5: Results of PCR. A: NIBV-SX9 strain S2 Gene amplified by PCR. Lane M: 2000 DNA Marker; Lane 1: Negative control; Lane 2: Amplification of NIBV-SX9-S2 gene fragment. B: PCR analysis of positive bacterium (DH5α) of the recombinant plasmid pET-SX9-S2 with P6 primer. Lane M : 2000 DNA Marker; Lane 1: Negative control; Lane2-6: Positive single colony. C: PCR analysis of positive bacterium (DH5α) of the recombinant plasmid pET-SX9-S2 with S2 primer. Lane M : 2000 DNA Marker; Lane 1: Negative control; Lane2-6: Positive single colony. D: PCR analysis of positive bacterium (BL21) of the recombinant plasmid pET-SX9-S2 with P6 primer. Lane M : 2000 DNA Marker; Lane 1: Negative control; Lane2-6: Positive single colony. E: PCR analysis of positive bacterium (BL21) of the recombinant plasmid pET-SX9-S2 with S2 primer. Lane M : 2000 DNA Marker; Lane 1: Negative control; Lane2-6: Positive single colony.

The results of S2 protein expression and purification: The His-tagged protein in the pET-His-32a (+) vector had a molecular mass of approximately 18 kDa, the S2 protein was 27 kDa and the expected fusion protein was about 45 kDa. The diagram of S2 protein expression is shown in Fig. 6A. As shown in Fig. 6B (lane 4), it was observed that the BL21 strain harboring the recombinant expression plasmid pET-SX9-S2, upon induction with IPTG, produced a protein band approximately 45 kDa in size, corresponding to the fusion protein of His and S2, designated as rHis-S2 protein. In contrast, the untransformed BL21, as well as BL21 strains transformed with either the pET-32a(+) vector or pET-SX9-S2 without IPTG induction, did not exhibit this protein band (refer to Fig. 6B, lanes 1 to 3). The analysis further revealed that the precipitate obtained post-ultrasonic disruption contained a substantial amount of the target protein (Fig. 6B, lane 6), whereas the supernatant contained only a minor quantity of soluble target protein (Fig. 6B, lane 5). These findings suggest that the recombinant expression plasmid pET-SX9-S2 in the bacteriophage predominantly expressed the rHis-S2 protein as inclusion bodies. The optimal conditions for protein expression were used for bulk protein expression, the precipitate was taken by sonication and the inclusion body proteins were purified by affinity chromatography on Ni2+ columns, which showed that there were few stray bands of proteins eluted by all gradients and good results were obtained by 100, 200, 300 and 400 mmol/ L imidazole elution (Fig. 6C, lane 6~9). The purified protein was dialyzed and concentrated to a concentration of approximately 2.4 mg/mL (Fig. 6D).

Preparation and titer detection of anti-NIBV-SX9-S2 polyclonal antibodies: Following the administration of both primary and booster immunizations to the experimental rabbits, blood samples were collected from the auricular vein for serum analysis. The serum titer of the S2 rabbit polyclonal antibody was subsequently evaluated using the standard indirect ELISA method, with purified rHis-S2 protein as the antigen. The findings revealed that at a dilution of 1:1,024,000, the rabbit polyclonal antibody demonstrated a P/N ratio of ≥2.1, indicating a titer exceeding 1:1,024,000 and the optimal titer of this polyclonal antibody was determined to be 1:32,000 (Fig. 7).

Expression of NIBV-SX9-S2 and ABCG2 in kidney of NIBV-infected chicks: Fig. 8A presents the Western blot results of NIBV-S2 and ABCG2 proteins in kidney tissues at 3, 6, 9, 12 and 15 dpi with NIBV. Analysis yielded the results depicted in Fig. 8B and 8C, demonstrate a progressive increase in NIBV-S2 expression from 3 to 6 dpi, reaching a peak at 9 dpi. In contrast, ABCG2 expression initially shows an upward trend at 3 dpi but is notably downregulated by 9 dpi. ABCG2, or adenosine triphosphate-binding cassette transporter G2, is predominantly localized in the proximal tubular epithelium of the kidney, where it facilitates the transport of uric acid from intracellular to extracellular compartments via ATP hydrolysis. Additionally, molecular docking analyses depicted in Fig. 8D reveal a strong binding affinity between the NIBV-S2 (green) protein and chicken ABCG2 protein (purple), ΔG=-48.1kcal/mol. This interaction may play a crucial role in NIBV's pronounced tropism for renal tiXssue.

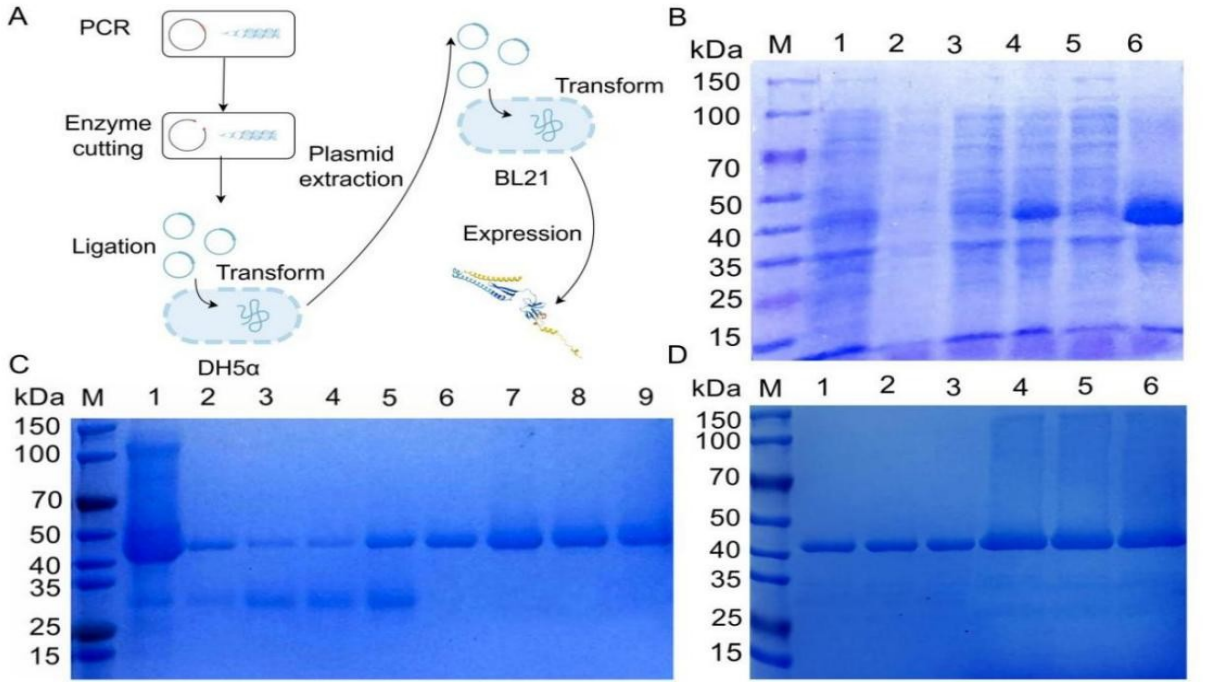

Fig. 6: Results of SDS-PAGE. A: Schematic Diagram of Prokaryotic Expression. B: Identification of rHis-S2 expression forms. Lane M: 180 protein Marker; Lane1: BL21 untransformed with pET-SX9-S2 has been treated with IPTG; Lane2: BL21 transformed with pET-32a(+) has been treated with IPTG; Lane3: BL21 transformed with pET-SX9-S2 without IPTG; Lane4: BL21 transformed with pET-SX9-S2 has been treated with IPTG; Lane 5: The supernatants of post-ultrasound sample. Lane 6: Sedimentation of post-ultrasound sample. C: Purification of rHis-S2 protein. Lane M: 180 protein Marker; Lane1: Unpurified sample; Lane 2-9: Elution results with 20, 30, 50, 80, 100, 200, 300 and 400 mmol/ L imidazole, respectively. D: Dialysis and concentration results of purified rHis-S2 protein. Lane M: 180 protein Marker; Lane 1~3: Dialysis results of purified rHis-S2 protein. Lane 4~6: Concentration results of purified rHis-S2 protein.

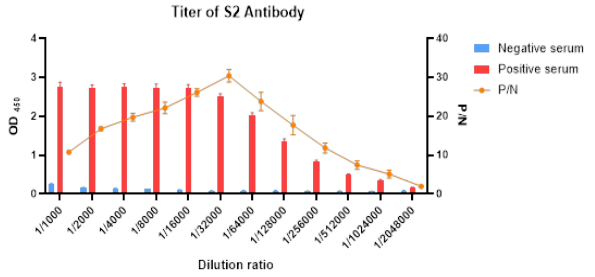

Fig. 7: Indirect ELISA titer determination of S2 antibody.

Interaction between S2 and ABCG2 *in-vitro* and *in-vivo:* To further elucidate correlation between the S2 protein and ABCG2, an immunofluorescence colocalization analysis of NIBV-S2 and ABCG2 was conducted on kidney tissue harvested at 9 days post-infection (9 dpi). As illustrated in Fig. 9A, the CK group exhibited no detectable NIBV-S2 (green) fluorescence signal, whereas the ABCG2 (red) signal was predominantly localized along the brush border of the proximal tubules in the kidneys. In contrast, following NIBV infection, distinct NIBV-S2 green fluorescence signals were observed, which were accompanied by a marked reduction in ABCG2 red fluorescence signals relative to the CK group. Moreover, there was significant colocalization of both signals, as indicated by the presence of yellow fluorescence.

The interaction between the S2 protein and ABCG2 was further examined using a co-immunoprecipitation (Co-IP) assay. As depicted in Fig. 9B, the antibody targeting the S2 protein successfully co-precipitated ABCG2 and reciprocally, the antibody against ABCG2 was able to co-precipitate S2. Following immuno-precipitation of S2, the expression level of ABCG2 in the NIBV group was observed to be lower than that in the control group. Conversely, after immunoprecipitation of ABCG2, the presence of the S2 protein was detectable in the NIBV group but was absent in the CK group. As shown in Fig. 9C, renal tubular epithelial cells were treated with the ABCG2 inhibitor Ko143. The findings indicated that post-NIBV infection, the expression level of ABCG2 in these cells was downregulated. Furthermore, continuous treatment with Ko143 led to a further reduction in ABCG2 expression levels, accompanied by a corresponding decrease in the expression level of the S2 protein.

MD simulations: The root-mean-square deviation (RMSD) and radius of gyration (Rg) analyses were conducted to evaluate the binding stability and compactness of the S2 and ABCG2 protein complex, respectively. The RMSD and Rg results demonstrated a gradual stabilization of the S2-ABCG2 complex as the simulation advanced (Fig. 10A and Fig. 10B). Root mean square fluctuations (RMSF) provide insights into the flexibility of proteins during molecular dynamics simulations. As illustrated in Fig. 10C, the RMSF values for the sequence segments were relatively low, suggesting a high degree of structural stability for the entire S2-ABCG2 complex. Furthermore, the binding conformation superposition analysis indicated a high degree of superimposition between the S2 and ABCG2 proteins (Fig. 10D). The free energy landscape diagram characterizes the lowest-energy conformations throughout the dynamic simulation of the complex structure. Analyses depicted in Fig. 10E and Fig. 9F revealed that the complex of S2 and ABCG2 proteins predominantly maintained a single, stable conformation, existing primarily in a low-energy state.

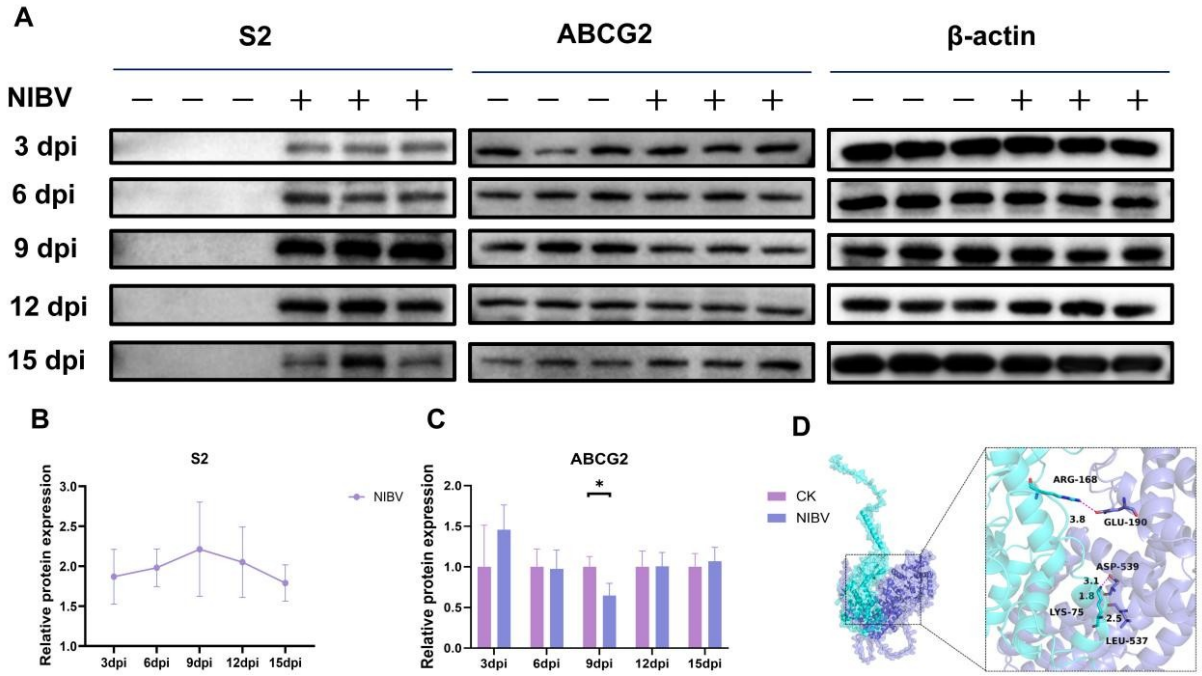

Fig. 8: The identification of alterations in NIBV-SX9-S2 and ABCG2 protein levels of kidney in chicks infected with NIBV. A:Western blot result of S2 and ABCG2 protein. B: Relative protein expression level of S2 protein. C: Relative protein expression level of ABCG2 protein. D: Molecular docking results of S2 and ABCG2 protein.

DISCUSSION

Infectious bronchitis virus (IBV), a γ-coronavirus, causes acute, highly contagious respiratory disease in poultry and can damage multiple organs in chickens, including the trachea, lungs, kidneys, glandular stomach, ovaries and oviduct (Zhang *et al*., 2025). Of particular concern is the nephropathogenic infectious bronchitis virus (NIBV), which can result in mortality rates of 30~50%, thereby posing a significant threat to the poultry industry (Li *et al*., 2025). Consequently, it is imperative to investigate the pathogenic mechanisms of NIBV in the kidneys to develop effective prevention and control strategies for infectious bronchitis.

The S protein of NIBV, a highly glycosylated virulence factor, is cleaved by host proteases at alkaline cleavage sites such as RRSRR, resulting in the formation of two subunits, S1 and S2 (Tian *et al*., 2023). Current research predominantly focuses on the S1 subunit, which is prone to mutations and recombination, whereas the role of the relatively conserved S2 protein in viral infectivity and pathogenicity remains to be fully understood (Nilo *et al*., 2022; Ali *et al*., 2025). Notably, the S2 protein is crucial for the fusion of the viral membrane with the host cell membrane, facilitating the efficient release of the viral genome into the host cell (Zhu *et al*., 2025). Furthermore, it is postulated that the S2 protein can interact with various factors, including proteins and lipid components within the host cell, potentially playing a specific role in the pathogenesis of coronaviruses (Li, 2016; Huang *et al*., 2020; Grunst *et al*., 2024). While studies have demonstrated that the cleavage site of the S protein is present in all IBV strains, there is currently no direct evidence linking the S2 protein to the histophilicity or pathogenicity of NIBV.

To explore the relationship between these factors, this study successfully constructed the pET-His-S2 recombinant expression plasmid for the first time, achieved prokaryotic expression of the recombinant NIBV-SX9-S2 protein and developed a rabbit polyclonal antibody against rHis-S2. The pET system is a prominent method for expressing foreign genes in E. coli, often yielding proteins that constitute up to 50% of the cell's total protein shortly after induction (He *et al*., 2018). In this study, the NIBV-SX9-S2 gene was cloned into the pET-32a(+) vector to create the pET-SX9-S2 plasmid, which was then transformed into BL21 cells for expression (Luo *et al*., 2025). Using IPTG as an inducer, strong promoter activity facilitated efficient protein production (Li *et al*., 2024; Chen, *et al*., 2025). SDS-PAGE confirmed that the recombinant rHis-S2 protein had a molecular weight of about 45 kDa, as expected and was mainly found in inclusion bodies. After solubilization, purification and renaturation, a high-purity rHis-S2 protein was obtained. This protein served as an antigen to generate high-titer, specific polyclonal anti-rHis-S2 antibodies in rabbits through multiple subcutaneous immunizations. This antibody was subsequently employed in western blot and immuno-fluorescence assays to facilitate further investigation.

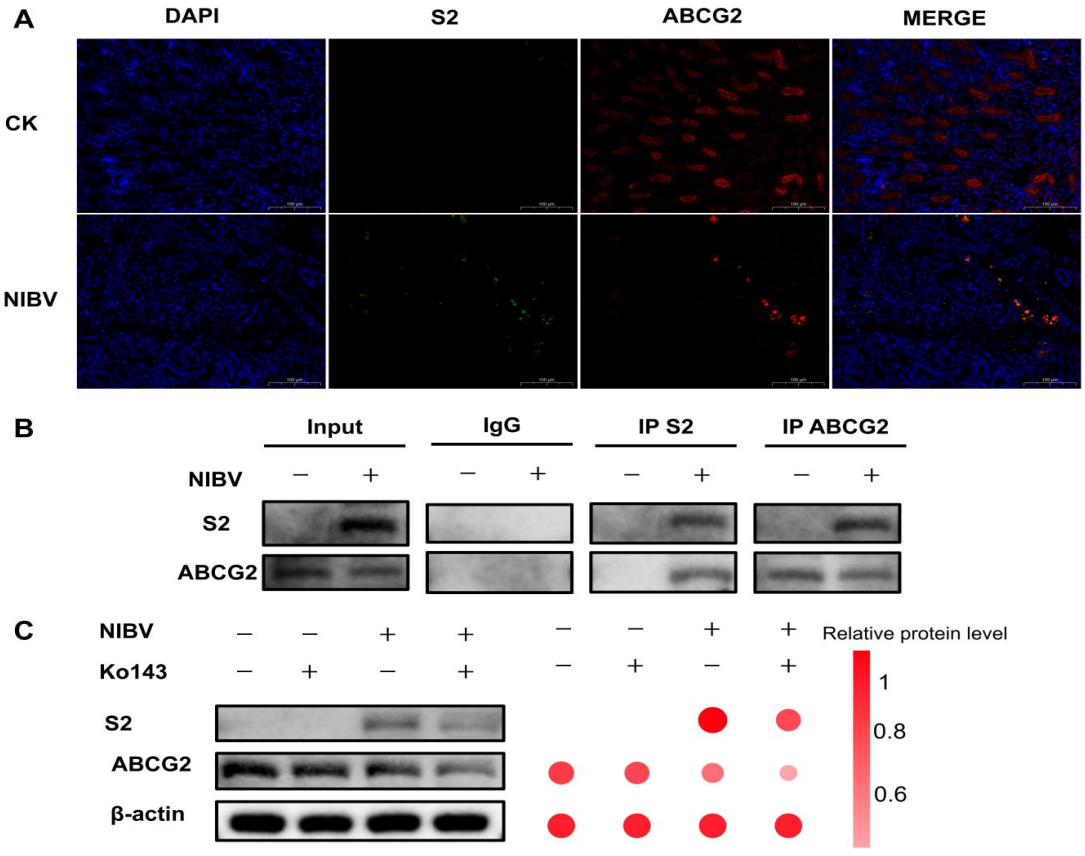

Fig. 9: Interaction between S2 and ABCG2 in the kidney tissue and renal tubular epithelial cells infected with NIBV. A: Co-localization of S2 and ABCG2 fluorescence B: Co-immunoprecipitation results of S2 and ABCG2. C: Treatment renal tubular epithelial cells with the ABCG2 inhibitor (Ko143).

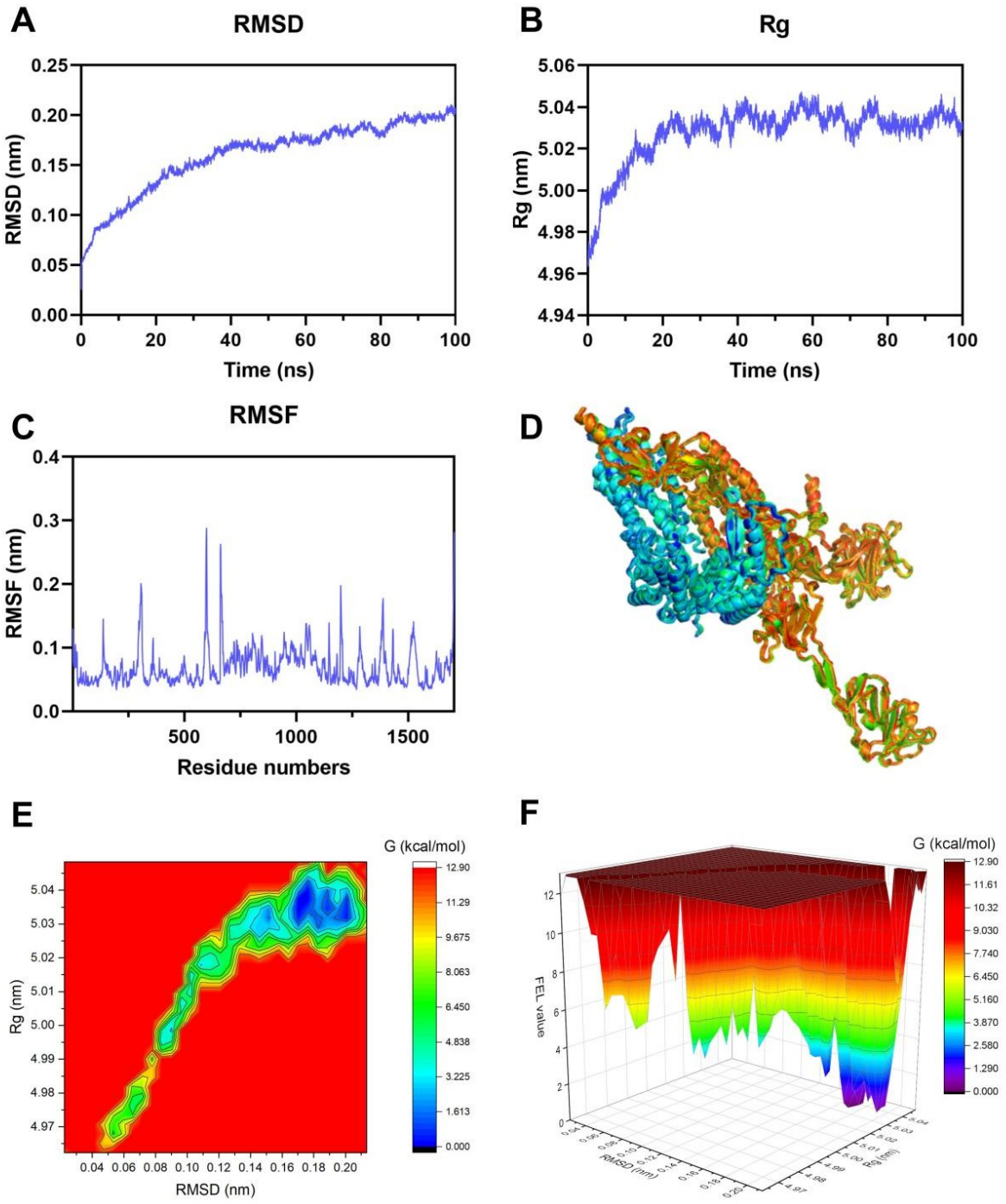

Fig. 10: Results of MD simulations analysis. A. RMSD analysis of complexes, S2 and ABCG2. B: Rg analysis of complexes, S2 and ABCG2. C: RMSF analysis of complexes, S2 and ABCG2. D: Simulated conformational superposition, S2 and ABCG2. E: X-Y graphs of free energy landscape analysis. F: X-Y-Z graphs of free energy landscape analysis.

The ABCG2 protein, a member of the ATP-binding cassette (ABC) superfamily, plays a crucial role in the transmembrane transport of various substrates, including uric acid (Han *et al*., 2025). This protein forms homodimers through a nucleotide-binding domain and a transmembrane region, functioning as a primary uric acid excretion protein in the kidney, with predominant expression in renal tubular epithelial cells and other locations (Eckenstaler & Benndorf, 2021). This study demonstrated that during the peak infection period (9 days post-infection, dpi), the expression of the ABCG2 protein was significantly downregulated in the group infected with NIBV compared to the control group, resulting in a marked impairment of renal uric acid excretion capacity, consistenting with the research results of Chen *et, al* (Chen, Shi, *et al*., 2025). This impairment may contribute to renal urate deposition. Additionally, the results indicated a significant increase in NIBV-S2 protein expression from 3 to 9 dpi, with a peak at 9 dpi. Therefore, we speculate that this protein was found to obstruct uric acid excretion pathways by binding to ABCG2.

To further substantiate the interaction between the S2 protein and the ABCG2 protein, we utilized co-immunoprecipitation (Co-IP) and molecular dynamics (MD) simulations. The Co-IP results demonstrated that the S2 protein antibody was capable of precipitating ABCG2 and reciprocally, the ABCG2 protein antibody could precipitate S2. The MD simulations indicated that S2 binds directly and stably to ABCG2 proteins, exhibiting multiple binding sites and interaction forces. To assess the role of ABCG2 in the regulation of S2, we employed Ko143 to inhibit ABCG2 expression in renal tubular epithelial cells. Following the application of the inhibitor, a significant downregulation of ABCG2 was observed, accompanied by a reduction in S2 protein expression levels. These findings suggest that ABCG2 may serve as a target for the action of the S2 protein. Aforementioned findings shows that NIBV potentially employs its S2 protein to recognize and bind to the ABCG2 protein in renal tissue. This interaction may facilitate viral colonization within the kidneys while concurrently disrupting the normal uric acid excretion pathway mediated by ABCG2. Such a dual effect could impair uric acid clearance, leading to substantial urate deposition within the renal tissue and ultimately culminating in the characteristic pathological changes known as "mottled kidney."

Conclusions: In conclusion, this study successfully amplified the coding gene for NIBV-S2 using RT-PCR and subsequently cloned it into the prokaryotic expression vector pET-32a(+), resulting in the construction of the recombinant expression plasmid pET-SX9-S2. This plasmid was then transformed into E. coli BL21 (DE3) to facilitate the expression of the rHis-S2 protein. The expressed rHis-S2 protein was employed to produce a polyclonal antibody, which demonstrated an indirect ELISA titer of up to 1:1,024,000. The rabbit polyclonal antibody against the NIBV-S2 protein developed in this study is effective for the detection of NIBV-S2. Moreover, empirical evidence indicates that NIBV-S2 exhibits a high binding affinity for the ABCG2 protein in renal tissues, along with the a marked downregulation of ABCG2 expression. This downregulation may contribute to substantial urate accumulation, thereby precipitating the characteristic pathological alterations.

Ethics approval and consent to participate: All animal protocols employed in this research, as well as all experimental procedures, were conducted in accordance with the guidelines established by requirements of the Animal Welfare and Ethics Committee of Jiangxi Agricultural University.

Conflicts of Interest: The authors declared no conflicts of interest.

Authors contribution: ZL, YS, XG, XG, CY conceived and designed the study; ZL, YS, MW, LQ performed the analysis of sera and tissue samples; ZL, CC, KZ, ML carried out the data analysis.

Acknowledgments: This work was supported by the National Key R&D Program of China (2023YFD1801100), the National Natural Science Foundation of China (32360906), the Technology System of Modern Agricultural Poultry Industry of Jiangxi Province (JXARS), the Key R&D Program of Jiangxi Province (20224BBF62003 and 20252BCF320013), the Natural Science Foundation of Jiangxi Province of China (20232ACB205013) and Graduate Student Innovation Project of Jiangxi Province (YC2025-B078).

REFERENCES

Ali A, Rahimi R, Mahmoud ME, *et al*., 2025. Genetic and phenotypic investigations of viral subpopulations detected in different tissues of laying hens following infectious bronchitis virus infection. Viruses 17(4). https://doi.org/10.3390/v17040527

An X, Xu Y, Mao Q, *et al*., 2025. Investigation of pharmacological mechanisms and active ingredients of cichorium intybus l. In alleviating renal urate deposition via lncrna h19/mir-21-3p regulation to enhance abcg2 expression. International Journal of Molecular Science 26(16):7892-7892. https://doi.org/10.3390/ijms26167892

Bernard D, Patrick G, Nicolas O, *et al*., 2022. Evidence of antibodies against SARS-CoV-2 in wild mustelids from Brittany (France). Transboundary Emerging Diseases 69(5):e3400-e3407. https://doi.org/10.1111/tbed.14663

Chen Y, Feng C, Huang C, *et al*., 2024. Preparation of polyclonal antibodies to chicken P62 protein and its application in nephropathogenic infectious bronchitis virus-infected chickens. International Journal of Biology and Macromolecules 271(P2):132515-132515. https://doi.org/10.1016/j.ljbiomac.2024.132515

Chen Y, Pan Y, Yu S, *et al*., 2025. Prokaryotic expression, polyclonal antibody production, and application of yak TGF-beta2. Animal Reproduction 22(4):e20250006. https://doi.org/10.1590/1984-3143-ar2025-0006

Chen Y, Shi Y, Huang C, *et al*., 2025. Nephropathogenic infectious bronchitis virus induces epithelial-mesenchymal transition of renal tubular epithelial cells through the TGF-beta/p-P38 pathway causing uric acid excretion disorder in chickens. Journal of Virology 99(11):e0103125. https://doi.org/10.1128/jvi.01031-25

Feng CL, Huang C, Shi Y, *et al*., 2023. Preparation of polyclonal antibodies to the chicken Beclin1 protein and its application in the detection of nephropathogenic infectious bronchitis virus. International Journal of Biology and Macromolecules 253(P8):127635-127635. https://doi.org/10.1016/j.ljbiomac.2023.127635

Eckenstaler R and Benndorf RA, 2021. The role of ABCG2 in the pathogenesis of primary Hyperuricemia and Gout-An update. International Journal of Molecular Science 22(13). https://doi.org/10.3390/ijms22136678

Fan S, Shen Y, Li S, *et al*., 2023. The S2 subunit of Infectious bronchitis virus affects abl2-mediated syncytium formation. Viruses 15(6). https://doi.org/10.3390/v15061246

Grunst MW, Qin Z, Dodero-Rojas E, *et al*., 2024. Structure and inhibition of SARS-CoV-2 spike refolding in membranes. Science 385(6710):757-765. https://doi.org/10.1126/science.adn5658

Han QQ, Ren QD, Guo X, *et al*., 2025. Punicalagin attenuates hyperuricemia via restoring hyperuricemia-induced renal and intestinal dysfunctions. Journal of Advanced Research 69:449-461. https://doi.org/10.1016/j.jare.2024.03.029

He T, Wang M, Cao X, *et al*., 2018. Molecular characterization of duck enteritis virus UL41 protein. Virology Journal 15(1):12. https://doi.org/10.1186/s12985-018-0928-4

Huang Y, Yang C, Xu XF, *et al*., 2020. Structural and functional properties of SARS-CoV-2 spike protein: potential antivirus drug development for COVID-19. Acta Pharmacol Sinica 41(9):1141-1149. https://doi.org/10.1038/s41401-020-0485-4

Jiang Y, Cheng X, Gao M, *et al*., 2024. Two mutations on S2 subunit were critical for Vero cell tropism expansion of infectious bronchitis virus HV80. Veterinary Microbiology 294:110134. https://doi.org/10.1016/j.vetmic.2024.110134

Li F, 2016. Structure, function, and evolution of coronavirus spike proteins. Annual Reviews in Virology 3(1):237-261. https://doi.org/10.1146/annurev-virology-110615-042301

Li N, Huang C, Chen W, *et al*., 2022. Nephropathogenic infectious bronchitis virus mediates kidney injury in chickens via the tlr7/nf-

κb signaling axis. Frontiers in Cellular and Infectious Microbiology 12:865283. https://doi.org/10.3389/fcimb.2022.865283

Li X, Xie Z, Wei Y, *et al*., 2024. Recombinant hemagglutinin protein from h9n2 avian influenza virus exerts good immune effects in mice. Microorganisms 12(8). https://doi.org/10.3390/microorganisms12081552

Li Y, Qi Q, Chen Y, *et al*., 2025. RIPK3 activation of CaMKII triggers mitochondrial apoptosis in NIBV-infected renal tubular epithelial cells. Veterinary Microbiology 302:110375. https://doi.org/10.1016/j.vetmic.2025.110375

Liu X, Chang X, Wu Q, *et al*., 2022. Lithium chloride inhibits infectious bronchitis virus-induced apoptosis and inflammation. Microbial Pathogenesis 162:105352. https://doi.org/10.1016/j.micpath.2021.105352

Loor-Giler A, Muslin C, Santander-Parra S, *et al*., 2025. Simultaneous detection and partial molecular characterization of five RNA viruses associated with enteric disease in chickens: chicken astrovirus, avian nephritis virus, infectious bronchitis virus, avian rotavirus a and avian orthoreovirus, via multiplex RT-qPCR. Frontiers in Veterinary Science 12:1536420. https://doi.org/10.3389/fvets.2025.1536420

Luo M, Shuai W, Guo Z, *et al*., 2025. Expression and immunological characterization of African Swine Fever Virus EP153R protein for serodiagnosis and its delivery via a recombinant PRRSV live vector. Vaccines (Basel) 13(11). https://doi.org/10.3390/vaccines13111110

Mani N, Suresh R and Chakraborty S, 2025. Cleaved versus uncleaved: How furin cleavage reshapes the conformational landscape of SARS-CoV-2 spike. Protein Science 34(12):e70368. https://doi.org/10.1002/pro.70368

Nilo I, Kazantzi FAS, Santos FF, *et al*., 2022. Emergence and molecular characterization of the avian infectious bronchitis virus GI-23 in commercial broiler farms from South America. Transboundary Emerging Diseases 69(6):3167-3172. https://doi.org/10.1111/tbed.14724

Qi Q, Li Y, Ding M, *et al*., 2024. Wogonin inhibits apoptosis and necroptosis induced by nephropathogenic infectious bronchitis virus in chicken renal tubular epithelial cells. International Journal of Molecular Science 25(15). https://doi.org/10.3390/ijms25158194

Rafique S, Jabeen Z, Pervaiz T, *et al*., 2024. Avian infectious bronchitis virus (AIBV) review by continent. Frontiers in Cellular and Infectious Microbiology 14:1325346. https://doi.org/10.3389/fcimb.2024.1325346

Shen J, Xu Q, Chen L, *et al*., 2023. Andrographolide inhibits infectious bronchitis virus-induced apoptosis, pyroptosis, and inflammation. Antiviral Therapy 28(5):13596535231207499. https://doi.org/10.1177/13596535231207499

Tian G, Huang C, Li Z, *et al*., 2023. Baicalin mitigates nephropathogenic infectious bronchitis virus infection-induced spleen injury via modulation of mitophagy and macrophage polarization in Hy-Line chick. Veterinary Microbiology 286:109891. https://doi.org/10.1016/j.vetmic.2023.109891

Uddin MM, Hasan A, Hossain I, *et al*., 2025. Molecular detection and epidemiological distribution of poultry respiratory viral pathogens in commercial chicken flocks in Bangladesh. Poultry Science 104(2):104679. https://doi.org/10.1016/j.psj.2024.104679

Xu G, Deng Y, Li Y, *et al*., 2024. S2 subunit plays a critical role in pathogenesis of TW-like avian coronavirus infectious bronchitis virus. Veterinary Microbiology 290:110010. https://doi.org/10.1016/j.vetmic.2024.110010

Yamada Y and Liu DX, 2009. Proteolytic activation of the spike protein at a novel RRRR/S motif is implicated in furin-dependent entry, syncytium formation, and infectivity of coronavirus infectious bronchitis virus in cultured cells. Journal of Virology 83(17):8744-8758. https://doi.org/10.1128/jvi.00613-09

You R, Liu K, Huang M, *et al*., 2023. Identification and comparison of the Sialic Acid-binding domain characteristics of Avian Coronavirus Infectious Bronchitis virus spike protein. Journal of Virology 97(5):e0048923. https://doi.org/10.1128/jvi.00489-23

Zhang B, Ding M, Zeng Y, *et al*., 2025. Nephropathogenic infectious bronchitis virus-induced pyroptosis of chicken renal tubular epithelial cells via the MDA5/NF-κB/NLRP3 signalling pathway. Veterinary Research 57(1):4. https://doi.org/10.1186/s13567-025-01651-4

Zhang J, Ren J, Wu W, *et al*., 2025. Emergence of novel QX-type IBV in China: molecular insights into unique S protein cleavage sites, antigenic drift, and enhanced pathogenicity (2025). BMC Veterinary Research 22:65. https://doi.org/10.1186/s12917-025-05224-7

Zhu Q, Liu T, Qin W, *et al*., 2025. BTG3 inhibits porcine epidemic diarrhea virus replication by promoting viral S2 protein degradation through the autophagy and proteasome pathways. Veterinary Microbiology 302:110402. https://doi.org/10.1016/j.vetmic.2025.110402